Journal of Heat and Mass Transfer Research

Journal homepage: https://jhmtr.semnan.ac.ir

Semnan University

ISSN: 2383-3068

Research Article

Natural Convection and Entropy Generation of Non-Newtonian Hybrid Cu-Al_2O_3/Water Nanofluid in an Inclined Partial Porous Cavity with Different Local Heater Positions in the Presence of Magnetic Field

Amin Kardgar [a] *

[a] *Department of Mechanical Engineering, Faculty of Engineering and Technology, University of Mazandaran, Babolsar, Iran*

ARTICLE INFO

Article history:

Received: 2023-05-14

Revised: 2023-12-25

Accepted: 2023-12-26

Keywords:

Hybrid Cu-Al2O3 nanofluid;

Partially porous media;

Position of heated wall;

Da number;

Porosity;

Non-Newtonian fluid.

ABSTRACT

In the present paper, natural convection of non-Newtonian hybrid Cu-Al2O3 nanofluid in an inclined partial porous cavity with changing heated wall position was numerically investigated. At first, the governing equations are rewritten non-dimensionally by utilizing dimensionless parameters. Then, the entropy generation equations are expressed in non-dimensional form. The discretization of governing equations is done by CVFVM (Control Volume Finite Volume Method). The coupling between pressure and velocity is handled by SIMPLE method and the obtained algebraic equations are computed by SIP solver. Nu number and irreversibility of flow and heat transfer are examined by main parameters such as Ha number, Da number, porosity, porous media thickness, position of heated wall, power law index and angle of inclination. Nu number increases almost 39%, 50% and 52% with enhancing porous media thickness from 0.1 to 0.6 at inclination angle of -30o, 0o and 30o, respectively. The Nu number increases by setting the hot surface at the lower part of the cavity. Nu decreases almost 10.5%, 7.6% and 5.2% by augmentation of Ha number from 0.0 to 40.0 at viscosity power law index of 0.6, 1.0 and 1.4, respectively. Nu increases almost 36%, 47% and 53% at inclination angle of 30o, 0o and −30o by enhancing volume fraction from 0.02 to 0.12, respectively. Convection heat transfer and fluid flow will be more dominant by augmentation of permeability and Da number and this will lead to more entropy generation by fluid flow and less entropy generation and irreversibility by magnetic field and convective heat transfer process. Fluid flow and magnetic field entropy generation decrease and heat transfer irreversibility and Be number rises by porous thickness ratio. Be number and thermal entropy generation increases with porosity. However, irreversibility due to magnetic field and flow friction decreases.

1. Introduction

Natural heat convection in porous media finds widespread applications in various industrial and engineering areas such as chemical processing, filtration, power technology, liquid food processing [1,2], petroleum industry [3-4], surgical implants, technology of drying (for textile materials and processing food grains), biological appliance, solar energy storage by phase change materials [5] and biomedical applications especially with non-Newtonian fluids. The use of nanofluids has attracted many

* **Corresponding author.**
E-mail address: a.kardgar@umz.ac.ir

Cite this article as:
Kardgar, A. 2023. Natural Convection and Entropy Generation of Non-Newtonian Hybrid Cu-Al2O3/Water Nanofluid in an Inclined Partial Porous Cavity with Different Local Heater Positions in the Presence of Magnetic Field, *Journal of Heat and Mass Transfer Research*, 10(2), pp. 279-300.

https://doi.org/10.22075/JHMTR.2023.30638.1442

attentions because the presence of nanofluids can increase thermal conductivity and heat transfer in the medium [6,7,8]. Comprehensive researches on the nanofluids are observable in the literature. Sheremet and Pop investigated nanofluid heat transfer in the tilted cavity with cold vertical wall [9]. A numerical study was conducted by Jamaludin et al. to elucidate the magnetohydrodynamic mixed convection of hybrid nanofluid [10]. Alsabery et al. studied the finite wall thickness effect in the enclosure filled with porous media. They concluded the convectional heat transfer can be impeded by the solid wall [11]. Khan et al. demonstrated that porous medium permeability, thermal buoyancy, the magnetic field and the heating element length has an essential effect in the improvement of Nu number [12]. Geridonmez and Oztop considered partial magnetic field in natural convection in the nanofluids [13]. They demonstrated the heat transfer can be more suppressed by the applying the magnetic field at the middle of the cavity. Porous media can weaken convectional heat transfer and strengthen conduction heat transfer. So, the application of porous media in cavity can have both positive and negative effect on the Nu number [14]. Rodríguez-Núñez et al. proposed a numerical model to investigated the unsteady natural convection in a cylinder in order to predict potential of the temperature distribution evolution in the aqueous silica [15]. Sheikholeslami and Vajravelu studied the effect of the Lorentz force on heat transfer with the variable magnetic field [16].

Zhang et al. numerically modeled the fluid flow and energy equation in a porous enclosure with moving wall by lattice Boltzmann method. They studied the internal heat source position on the Nu number [17]. Sheremet and Pop analysed the problem by Tiwari and Das' nanofluid model [18]. Li et al. used LB method to investigate the effect of Lorentz force on heat transfer [19]. Rajarathinam et al. investigated the mixed convection in an inclined cavity with upper and bottom wall moving oppositely. They concluded that the direction of the moving wall has significant role on the flow and heat transfer [20]. The MHD flow around a permeable triangle body in square cavity filled with Alumina nanofluid was examined by Lattice Boltzmann Method [21]. It was observed that the enhancement of permeability augments the fluid momentum, whereas the magnetic force declines the fluid kinetic energy. Gibanov et al. worked on ferrofluid heat transfer characteristics in cavity by performing a numerical modeling by considering the uniform horizontal magnetic field [22]. Rahmat Ellahi et al. investigated nanofluid flow in vertical wavy cone and pipe with analytic solution [23,24].

The phenomenon of buoyancy-driven natural convection in a porous media is extensively under investigation. Aneja et al. carried out an investigation to investigate heat transfer in Casson fluid numerically [25]. Astanina et al. analyzed the heat transfer in an open trapezoidal enclosure. They found that an Hartmann number enhancement can lead to a increment of amplitude of oscillations for average Nu and irreversibility [26]. Selimefendigil and Öztop calculated the influence of corrugation on heat transfer in U-shaped vented cavity. Their research demonstrated that the bottom wall corrugation which was a wave with triangular shape is an effective tool for fluid flow and heat transfer features [27]. Khan et al. [28] and Zeeshan et al. [29] studied darcy- Forchheimer flow. They concluded an increase in thermophoresis parameter and Schmidt number results in a decrease in concentration of nanoparticles.

Most researches on fluid flow in porous media have applied and still utilize the Darcy model to calculate the pressure drop with the superficial velocity [30, 31]. The boundary and inertia effects of the flow must be captured if the fluid velocity is relatively high. Previous investigations elucidated that the steady state Darcy model is adequate to simulate flow in saturated porous media, especially for low porosity media and low velocity flow. However, in order to accommodate different conditions the extended Darcy model is utilized in many studies. For example, Forchheimer and Brinkman extended model is extensively applied to capture non-linearity of porous matrix drag at high velocity [32].

It is apparent that there has been a significant oversight in the investigation of entropy generation within a partial porous enclosure, based on the existing literature review. The identification of key factors affecting entropy generation holds the potential to augment the sustainability, efficiency, and overall performance of thermodynamic processes and systems. Furthermore, a more in-depth analysis of entropy generation concerning parametric effects in natural convection can suggest valuable solutions to different engineering, renewable systems, and environmental challenges. Therefore, this research initiatively targets to explore the fundamental factors contributing to entropy generation in a parametric study of natural convection within a partial porous cavity subjected to a uniformly acting magnetic field. Additionally, a mathematical model based on the Darcy-Forchheimer-Brinkmann framework has been numerically simulated using the finite volume approach. CVFVM was employed to discretize partial differential equations of Navier-Stokes and energy equations. This investigation

will extensively discuss the essential components responsible for volumetric entropy generation, including irreversibilities arising from heat transfer, magnetic field and fluid friction effects. Furthermore, thoroughly exploring the Bejan number associated with each entropy generation component will provide valuable insights into the effect of individual irreversibility factors.

2. Theory and physics of the problem

The Physics of the problem and the computational domain is illustrated in Fig. 1. This is an inclined rectangular cavity partially filled with porous matrix with thickness of δ. The hybrid Cu/Al_2O_3 water nanofluid is influenced by the external magnetic field. The Rayleigh number range selected in the present work keeps the nanofluid flow two-dimensional and laminar. The right vertical wall of the cavity is kept at constant temperature TH, while the left vertical wall is maintained at constant cold temperature TC. The top and bottom horizontal wall is kept adiabatic. The following assumptions are considered in the study:

a) The flow is considered incompressible, laminar and steady.

b) Thermal non-equilibrium condition is between solid matrix and nanofluid.

c) The Darcy model and the Boussinesq approximation are applied.

d) The properties of the nanofluid and the porous medium are assumed homogeneous and isotropic,

e) In comparison with the external magnetic field, the induced magnetic field can be ignored.

f) The walls of cavity are considered impermeable.

2.1. Mathematical Modeling

By taking into account the afore-said assumptions, the coupled non-linear PDE's for mass continuity, momentum and energy are [33]:

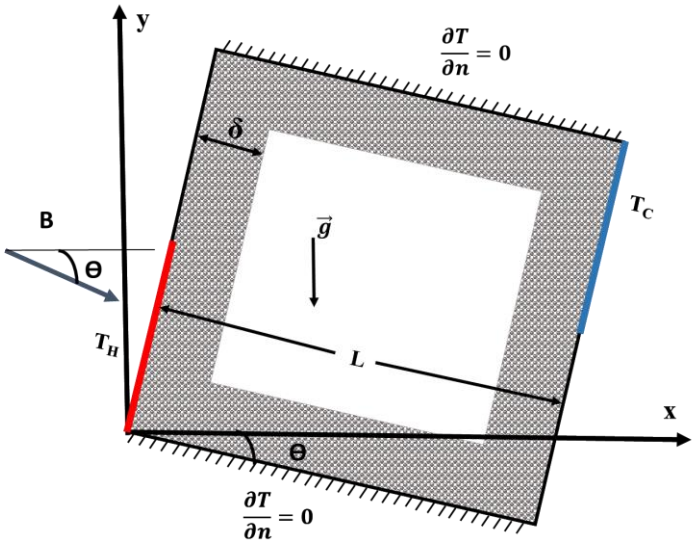

Fig. 1. The geometry of the problem with physical model and boundary conditions

Continuity
$$\frac{\partial u^*}{\partial x^*} + \frac{\partial v^*}{\partial y^*} = 0 \tag{1}$$

Momentum-x
$$\frac{\rho_{nf}}{\varepsilon^2}\left(\frac{\partial (u^* u^*)}{\partial x^*} + \frac{\partial (u^* v^*)}{\partial y^*}\right) = -\frac{\partial p^*}{\partial x^*} + \frac{\mu_{nf}}{\varepsilon}\left(\frac{\partial}{\partial x^*}\left(\frac{\partial u^*}{\partial x^*}\right) + \frac{\partial}{\partial y^*}\left(\frac{\partial u^*}{\partial y^*}\right)\right) - \frac{\mu u}{\rho_{hnf} K} + \sigma_{nf} B^2 (v^* sin\theta cos\theta - u^* sin^2\theta) - (\rho\beta)_{nf} g_x (\bar{T} - T_C) \tag{2}$$

Momentum-y
$$\frac{\rho_{hnf}}{\varepsilon^2}\left(\frac{\partial (u^* v^*)}{\partial x^*} + \frac{\partial (v^* v^*)}{\partial y^*}\right) = -\frac{\partial p^*}{\partial y^*} + \frac{\mu_{hnf}}{\varepsilon}\left(\frac{\partial}{\partial x^*}\left(\frac{\partial v^*}{\partial x^*}\right) + \frac{\partial}{\partial y^*}\left(\frac{\partial v^*}{\partial y^*}\right)\right) - \frac{\mu v}{\rho_{hnf} K} + \sigma_{hnf} B^2 (u^* sin\theta cos\theta - v^* cos^2\theta) - (\rho\beta)_{hnf} g_y (\bar{T} - T_C) \tag{3}$$

Fluid Energy
$$\varepsilon(\rho c_p)_{hnf}\left(\frac{\partial(u^*T_f{}^*)}{\partial x^*}+\frac{\partial(v^*T_f{}^*)}{\partial y^*}\right)=\varepsilon k_{hnf}\left(\frac{\partial}{\partial x^*}\left(\frac{\partial T_f{}^*}{\partial x^*}\right)+\frac{\partial}{\partial y^*}\left(\frac{\partial T_f{}^*}{\partial y^*}\right)\right)+h_v(T_s{}^*-T_f{}^*) \quad (4)$$

Solid Energy
$$0=(1-\varepsilon)k_s\left(\frac{\partial}{\partial x^*}\left(\frac{\partial T_s{}^*}{\partial x^*}\right)+\frac{\partial}{\partial y^*}\left(\frac{\partial T_s{}^*}{\partial y^*}\right)\right)-h_v(T_s{}^*-T_f{}^*) \quad (5)$$

The viscosity μ_{hnf}, the density ρ_{hnf}, the thermal capacity $(\rho c_p)_{hnf}$, and the coefficient of thermal expansion $(\rho\beta)_{hnf}$ are computed by the following formulas, respectively.

$$\mu_{hnf}=\frac{\mu_f}{(1-\varphi_1)^{2.5}(1-\varphi_2)^{2.5}} \quad (6)$$

$$(\rho c_p)_{hnf}=(1-\varphi_2)\left((1-\varphi_1)\rho_f c_{pf}+\varphi_1\rho_{n1}c_{pn1}\right)+\varphi_2\rho_{n2}c_{pn2} \quad (7)$$

$$(\rho\beta)_{hnf}=(1-\varphi_2)\left((1-\varphi_1)\rho_f\beta_f+\varphi_1\rho_{n1}\beta_{n1}\right)+\varphi_2\rho_{n2}\beta_{n2} \quad (8)$$

$$\rho_{hnf}=(1-\varphi_2)\left((1-\varphi_1)\rho_f c_{pf}+\varphi_1\rho_{n1}c_{pn1}\right)+\varphi_2\rho_{n2}c_{pn2} \quad (9)$$

$$\frac{k_{nhf}}{k_{bf}}=\frac{k_{n2}+2k_{bf}-2\varphi_2(k_{bf}-k_{n2})}{k_{n2}+2k_{bf}+\varphi_2(k_{bf}-k_{n2})} \quad (10)$$

$$\frac{k_{bf}}{k_f}=\frac{k_{n1}+2k_f-2\varphi_1(k_f-k_{n1})}{k_{n1}+2k_f+\varphi_1(k_f-k_{n1})} \quad (11)$$

$$\frac{\sigma_{nhf}}{\sigma_{bf}}=\frac{\sigma_{n2}+2\sigma_{bf}-2\varphi_2(\sigma_{bf}-\sigma_{n2})}{\sigma_{n2}+2\sigma_{bf}+\varphi_2(\sigma_{bf}-\sigma_{n2})} \quad (12)$$

$$\frac{\sigma_{bf}}{\sigma_f}=\frac{\sigma_{n1}+2\sigma_f-2\varphi_1(\sigma_f-\sigma_{n1})}{\sigma_{n1}+2\sigma_f+\varphi_1(\sigma_f-\sigma_{n1})} \quad (13)$$

in above the equations, the solid nanoparticle volume fraction is denoted by φ and subscript hnf, n and f stands for hybrid nanofluid, solid nanoparticle and base fluid, respectively. The fluid viscosity is

$$\mu_f=N\left\{2\left[\left(\frac{\partial u}{\partial x}\right)^2+\left(\frac{\partial v}{\partial y}\right)^2\right]+\left(\frac{\partial v}{\partial x}+\frac{\partial u}{\partial y}\right)^2\right\}^{\frac{n-1}{2}}$$

where N is the consistency coefficient and n is the power-law index.

The convection heat transfer coefficient between solid matrix and fluid is determined by the following relation[34].

$$h_v=\frac{Nuk}{d} \quad (14)$$

$$Nu=(1+0.99(RePr)^{0.66})\varepsilon^{1.79} \quad (15)$$

In the above relations, dimensional temperature, pressure, y-velocity and x-velocity are denoted by T^*, p^*, v^* and u^* respectively. The no-slip BC for velocity near wall and zero gradient for insulated wall and fixed temperature for right and left wall can be applied by the following equations:

Upper outer wall
$$y^*=L, 0\le x^*\le L, \frac{\partial T^*{}_s}{\partial y^*}=0 \quad (16)$$

Lower outer wall
$$y^*=0, 0\le x^*\le L, \frac{\partial T^*{}_s}{\partial y^*}=0 \quad (17)$$

Left outer wall
$$x^*=0, L/2\le y^*\le L, T^*=T_H \quad (18)$$

Right outer wall
$$x^*=L, L/2\le y^*\le L, T^*=T_C \quad (19)$$

Exergy is a thermodynamic concept, used for many years within engineering analyses of chemical and mechanical processes and systems. Officially, in thermodynamics, the exergy of a system is construed as the maximum potential of work of a component or system in a specified environment at a given state. The exergy destruction rate is proportional to the production of entropy. Irreversibilities can destroy exergy completely or partially in actual cycles and processes. In the studied problem, the exergy destruction is due to magnetic field, heat transfer and fluid flow. The rate of entropy generation due to fluid flow S_F^*, heat transfer S_T^* and magnetic field S_G^* can be formulated as follows [35]:

$$S_F^* = \frac{\mu_{hnf}}{T_0}\left[2\left(\frac{\partial u^*}{\partial x^*}\right)^2 + 2\left(\frac{\partial v^*}{\partial y^*}\right)^2 + \left(\frac{\partial u^*}{\partial y^*} + \frac{\partial v^*}{\partial x^*}\right)^2\right] \quad (20)$$

$$S_T^* = \frac{k_{hnf}}{{T_0}^2}\left[\left(\frac{\partial T^*}{\partial x^*}\right)^2 + \left(\frac{\partial T^*}{\partial y^*}\right)^2\right] \quad (21)$$

$$S_G^* = \frac{\sigma_{hnf} B^2}{T_0}(u^* sin\theta - v^* cos\theta)^2 \quad (22)$$

The total entropy generation can be achieved by summing up the aforementioned irreversibility as follows:

$$S_S^* = S_F^* + S_T^* + S_G^* \quad (23)$$

One the important non-dimensional number in MHD flow investigation is Bejan number which can be computed as:

$$Be = \frac{S_T^*}{S_S^*} \quad (24)$$

2.2. Numerical Procedure

Finite volume method (FVM) are utilized to discretize governing PDE's. The collocated arrangement of mesh is applied and in order to deal with velocity and pressure coupling the entrenched SIMPLE technique is employed with using the Rhie and Chow's momentum interpolation method [36]. X-momentum convective fluxes through right-face(e-face) of control volume demonstrated in Fig. 2 can be calculated as [37]:

$$F_e^c = \dot{m}_e u_e$$
$$u_e = (\rho u)_e \Delta y$$
$$F_e^c = \begin{cases} \max(\dot{m}_e, 0)u_P + \min(\dot{m}_e, 0)u_E \\ \dot{m}_e(1-\lambda_e)u_P + \dot{m}_e\lambda_e u_E \end{cases} \quad (25)$$
$$\lambda_e = \frac{x_e - x_P}{x_E - x_P}$$

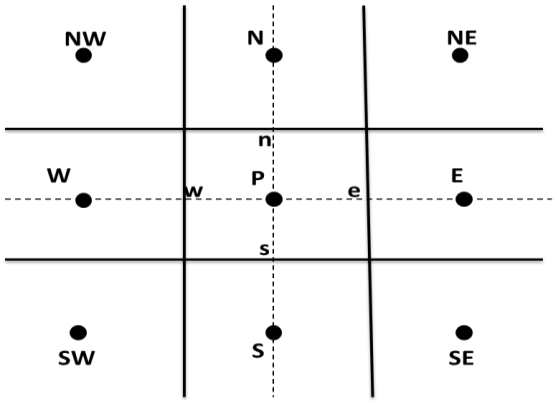

Fig. 2. Control volume and its north, south, west and east neighborhoods in the collocated arrangement of grid [37]

The same equations for other faces is obtained by applying central and upwind discretization scheme. For instance, the resulted equations for upwind scheme is as follow:

$$A_E^c = \min(\dot{m}_e, 0), \quad A_W^c = \min(\dot{m}_w, 0)$$
$$A_N^c = \min(\dot{m}_n, 0), \quad A_S^c = \min(\dot{m}_s, 0) \quad (26)$$
$$A_P^c = -(A_E^c + A_W^c + A_N^c + A_s^c)$$

By applying the central discretization scheme, the coefficient of convective fluxes in algebraic equations are:

$$A_E^c = \dot{m}_e\lambda_e, \quad A_W^c = \dot{m}_w\lambda_w$$
$$A_N^c = \dot{m}_n\lambda_n, \quad A_S^c = \dot{m}_s\lambda_s \quad (27)$$
$$A_P^c = -(A_E^c + A_W^c + A_N^c + A_s^c)$$

The equation for A_P^c is resulted from the continuity condition:

$$\dot{m}_e + \dot{m}_w + \dot{m}_n + \dot{m}_s = 0 \quad (28)$$

The diffusion terms is discretized by central differencing due to its physics. The coefficients are computed by the following relations:

$$F_e^d = \left(\mu\frac{\partial u}{\partial x}\right)_e \Delta y = \frac{\mu_e S_e}{x_E - x_P}(u_E - u_P)$$
$$A_E^d = -\frac{\mu_e S_e}{x_E - x_P}, \quad A_W^d = -\frac{\mu_w S_w}{x_P - x_W} \quad (29)$$
$$A_N^d = -\frac{\mu_n S_n}{x_N - x_P}, \quad A_S^d = -\frac{\mu_s S_s}{x_P - x_S}$$

Kholsa and Rubin [38] is applied to avoid diagonally domination in system of algebraic equations resulted from central differencing approximation. Because, system of algebraic equations with diagonally domination may diverge.

$$F_e^c = \dot{m}_e u_e^{UDS} + \dot{m}_e[u_e^{CDS} - u_e^{UDS}]^{m-1} \quad (30)$$

in which superscripts, CDS and UDS means central and upwind discretization scheme,

respectively. The last term in bracket is computed from former iteration and will vanish at convergence and the precision is analogous to CDS whilst the rate of convergence is like UDS [38].

The pressure term can be dealt like a source term in the momentum equation and is calculated as [39]:

$$Q_P^u = -(p_e S_e - p_w S_w)^{m-1} \tag{31}$$

The pressure treatment in order to avoid the checker board problem in collocated grid is expressed in [38]. The system of algebraic equations is obtained by rearranging the above relations:

$$\begin{aligned} &A_P^u u_P + A_E^u u_E + A_W^u u_W + A_N^u u_N + A_S^u u_S = Q_P^u \\ &A_E^u = A_E^c + A_E^d, \qquad A_W^u = A_W^c + A_W^d \\ &A_N^u = A_N^c + A_N^d, \qquad A_S^u = A_S^c + A_S^d \\ &A_P^u = A_P^t - (A_E^u + A_W^u + A_N^u + A_S^u) \\ &Q_P^u = Q_u^P + Q_u^c + Q_u^t \end{aligned} \tag{32}$$

where Q_u^c is:

$$Q_u^c = [(F_u^c)^{UDS} - (F_u^c)^{CDS}]^{m-1} \tag{33}$$

The systems of linear algebraic equations are solved by the Stone's SIP solver. Stone's scheme, also is well-known as SIP[1], is an algorithm developed for systems of equations resulting from the discretization of partial differential equations. The Biggest disadvantage of LU method is ignoring the advantage of coefficient matrix. So, Stone's method accelerate the convergence rate by considering a preconditioner matrix.

3. Grid Independency and Validation

The discretization of the governing equations was done by Finite volume method (FVM). A numerical code was developed in FORTRAN compiler to solve the resulted linear equations. An iterative procedure is adopted to obtain the converged solution. Therefore, the convergence criteria is considered to stop the iteration:

$$\left|\frac{\theta_{i,j} - \theta_{i,j}^{old}}{\theta_{i,j}}\right| < 10^{-10} \tag{34}$$

where θ may stand for velocity or temperature. Under relaxation number is considered 0.7 and 0.4 for velocity and for pressure, respectively.

Mesh independence is checked by using different grid sizes in the simulation domain. The results are seen in Fig. 3.

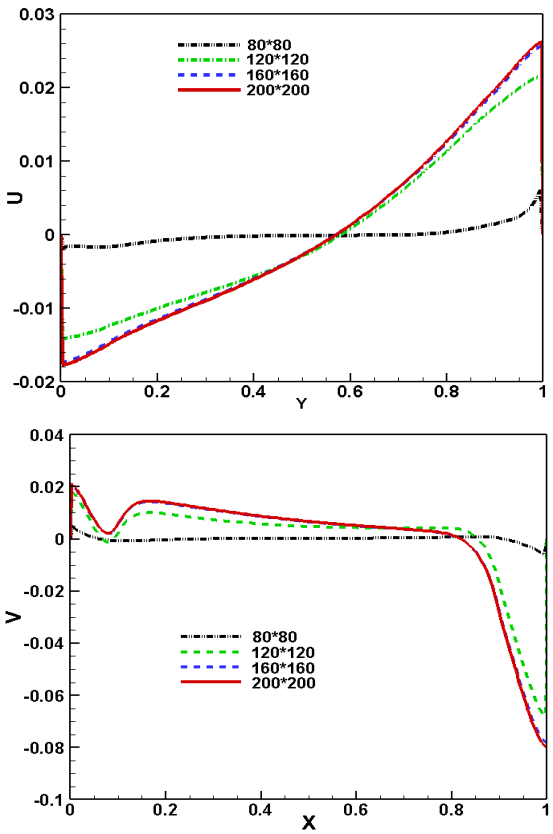

Fig. 3. U-velocity on vertical axis and V-velocity on horizontal axis with different number of meshes

Grid independent solution was achieved by 200*200 meshes. The domain with the generated grid is demonstrated in Fig. 4.

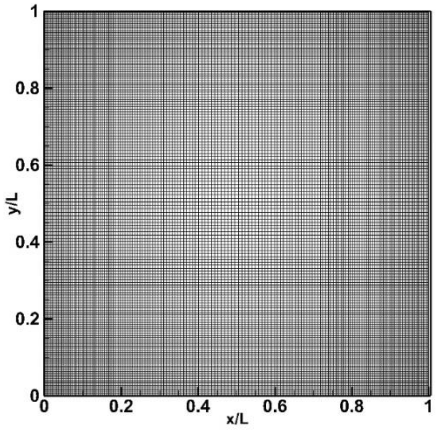

Fig. 4. Sample of the uniform structured mesh used for simulation

The present code has been verified successfully against the works of Khanafer et al. [40]. The present code result a in close agreement with numerical simulation of Khanafer et al. [40].

[1] Strongly Implicit Procedure

The comparison is concerned with u-velocity, v-velocity and temperature along the centerline. For more confident, the prepared numerical code was also verified against the experimental work of Krane and Jessee [41] with natural convection in a cavity with air as fluid in Fig. 6. There is a good agreement between numerical simulation and experimental result.

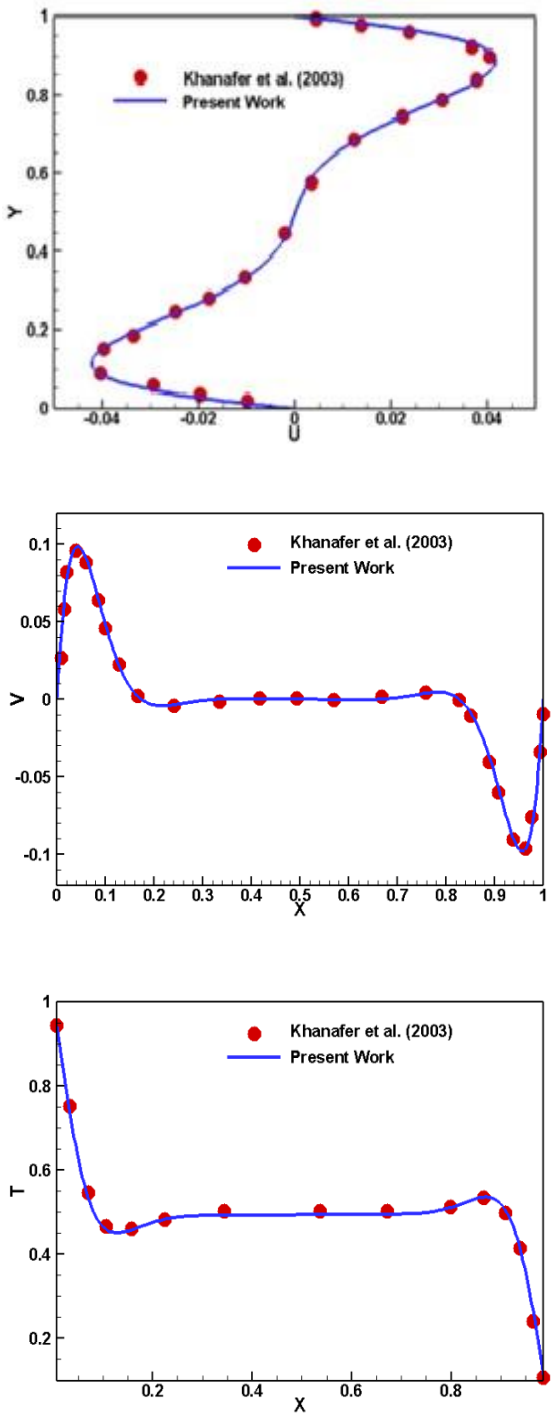

Fig. 5. Comparison between numerical results of Khanafer et al. [40] and present work for the temperature, U-velocity and V-velocity distribution on centerline at Gr=10^5, Pr=6.2 and φ=5%

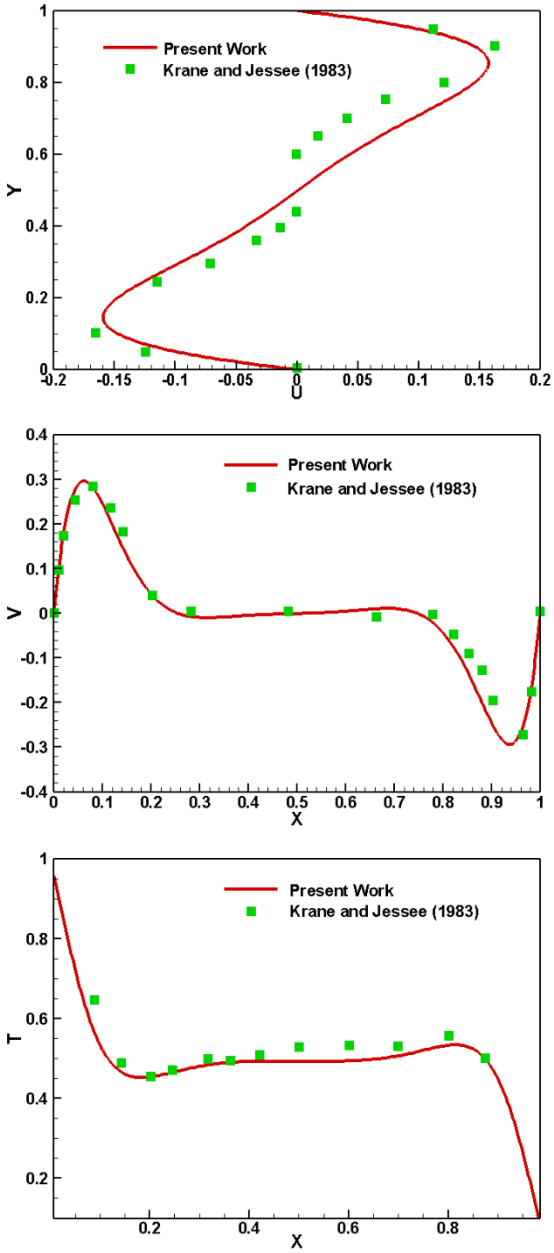

Fig. 6. Comparison between Krane and Jessee [41] experimental results and present work for the temperature, U-velocity and V-velocity distribution on centerline at Ra=1.89×10^5 and Pr=0.71

4. Results and Discussion

A numerical simulation has been performed to investigate the effects of different involved parameters in the present study, such as Rayleigh number Ra, Darcy number Da, porosity ε, porous media thickness, power law index, Hartman number Ha and volume fraction of nanofluid on natural convection of non-Newtonian fluid flow in the cavity partially filled with a porous media.

The effects of Da number on the averaged Nusselt at φ=0.05, δ/L=0.2, Ra=$1.5*10^6$ and ε=0.75 are explained in Fig. 7. As shown in the Figure, Nu enhances by increasing Da number. The augmentation of Nu number is more precipitous at Da greater than 10^{-4}. This is owing

to increasing the porous medium permeability and accordingly the severe fluid flow which causes the enhancing the convective heat from the hot wall.

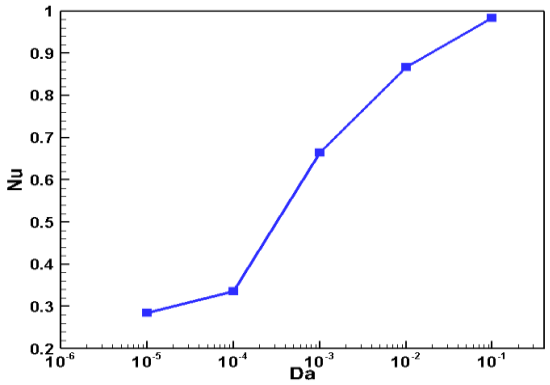

Fig. 7. The Nu number variation vs. Da number at δ/L=0.2, φ=0.05, Ra=1.5*106 and ε=0.75

Table 1. The Nu number variation vs. Da number at δ/L=0.2, φ=0.05, Ra=1.5*10⁶ and ε=0.75

Da	10^{-5}	10^{-4}	10^{-3}	10^{-2}	10^{-1}
Nu	0.284	0.336	0.664	0.867	0.983

The isotherm lines at different Da numbers are compared at Fig. 8. The isotherm lines get more dense and perpendicular to the hot wall by increasing the Da number and results in the temperature gradients enhancement and this will lead to Nu number increase.

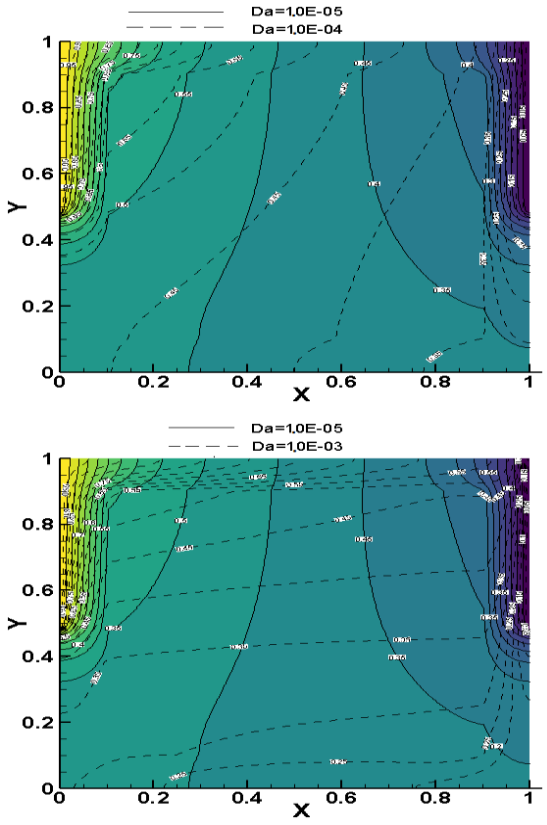

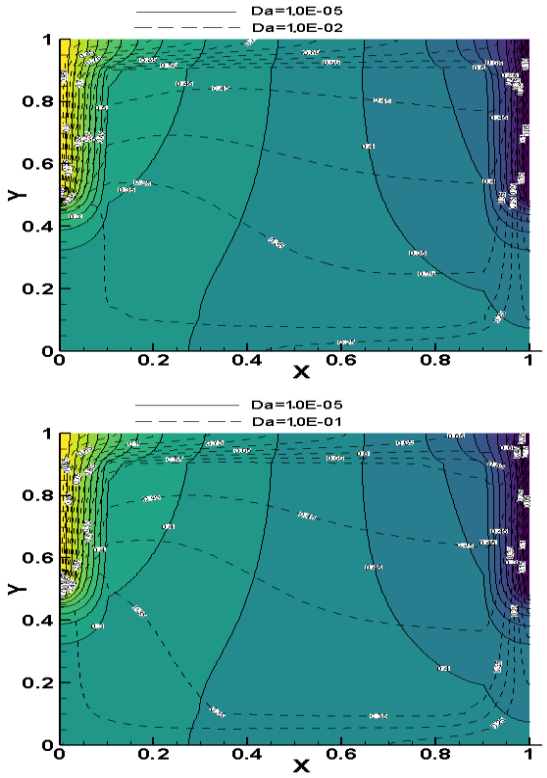

Fig. 8. Comparison of the isotherm lines at different Da numbers for φ=0.05, δ/L=0.2, Ra=1.5*106 and ε=0.75

To investigate the impact of porous media thickness and the angles of inclination on Nu number and heat transfer performance Fig. 9 is presented at φ=0.05, Ra=1.5*10⁶ and ε=0.75. According to Fig. 9, Nu increase almost 39%, 50% and 52% with enhancing porous media thickness from 0.1 to 0.6 at inclination angle of -30°, 0° and 30°, respectively.

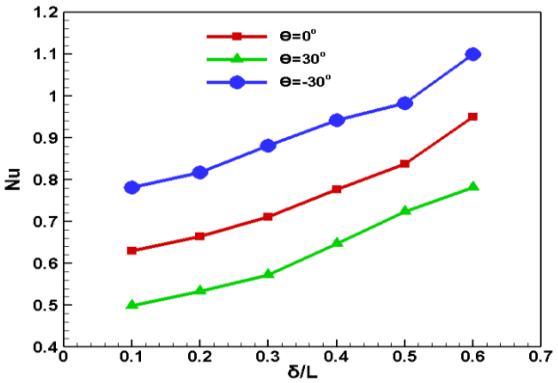

Fig. 9. The variation of the Nu number vs. porous media thickness at different angles of inclination at for φ=0.05, Ra=1.5*106, ks/kf=67 and ε=0.75

As can be seen in Fig. 10, increasing porous media thickness δ/L substantially weakens natural convection heat transfer and convection field is confined in non-porous region. However, by comparing the isotherm lines of δ/L=0.1 and δ/L=0.5, the isotherm lines become more uniform which indicates the dominance of conduction heat transfer mechanism at higher

thicknesses. Dominance of conduction heat transfer will lead to Nu increment due to high value of conductivity ratio. The Nu reduces with enhancement of inclination angle from −30° to +30°. With increasing the inclination angle, the gravitational component will reduce and consequence the buoyancy force reduction and Nu number decline.

Table 2. The variation of the Nu number vs. porous media thickness at different angles of inclination at for φ=0.05, Ra=1.5*10⁶, k_s/k_f=67 and ε=0.75

δ/L	0.1	0.2	0.3	0.4	0.5	0.6
Nu (θ=0°)	0.782	0.816	0.881	0.942	0.982	1.151
Nu (θ=30°)	0.633	0.664	0.711	0.777	0.838	0.951
Nu (θ=-30°)	0.499	0.534	0.572	0.647	0.723	0.781

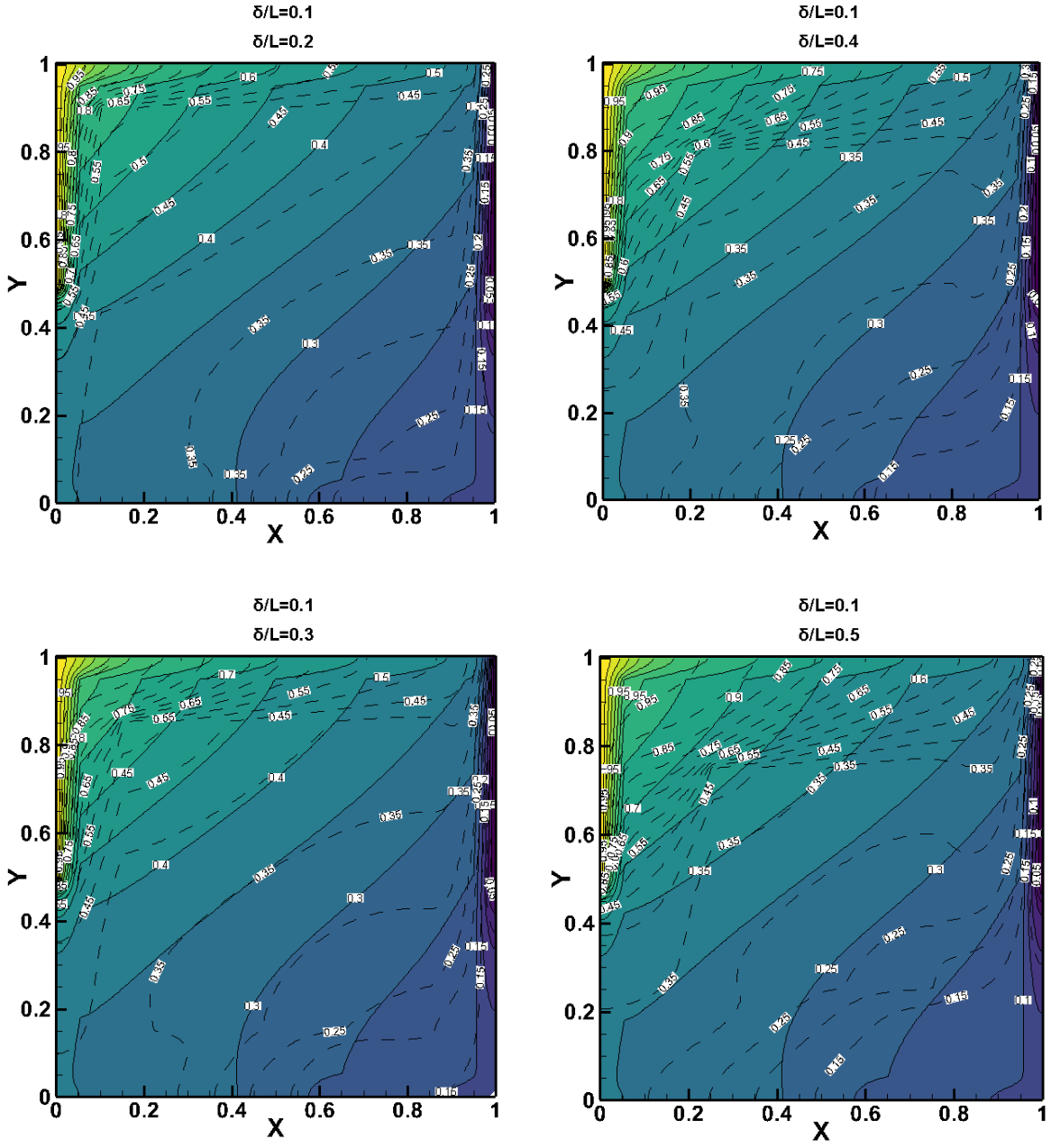

Fig. 10. Comparison of the isotherm lines at different porous media thicknesses for φ=0.05, Da=0.001, Ra=1.5*10⁶ and ε=0.75

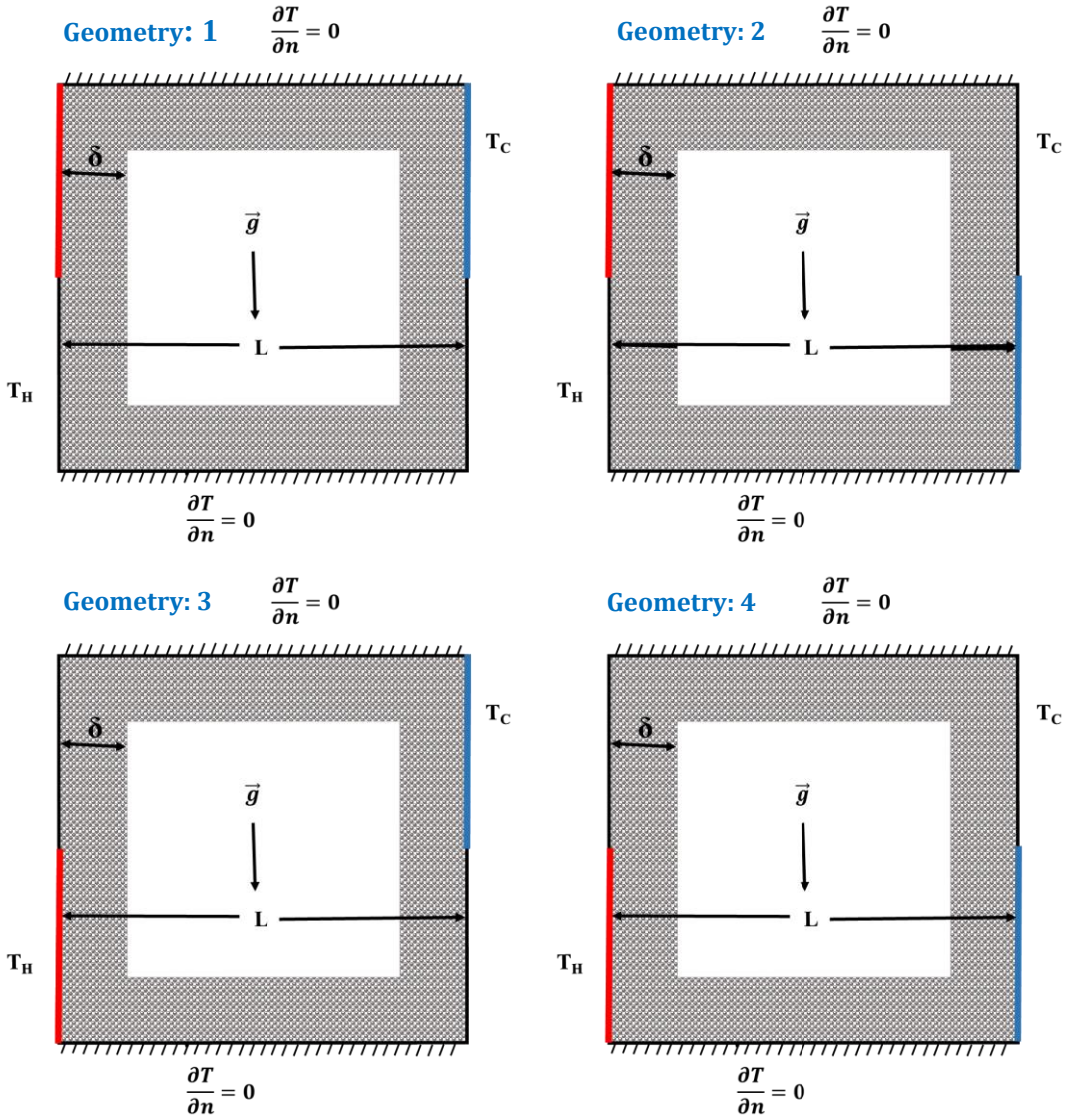

Fig. 11. The different arrangements of hot and cold sections in the cavity

The Nu number variation versus volume fraction of nanofluid at different geometries (Fig. 11) is depicted in Fig. 12. Nu linearly enhances by increasing volume fraction of nanoparticle at different location of hot and cold surfaces. Thermal conductivity of nanofluid augments with increment of nanoparticle volume fraction and leads in Nu number rise.

The Nu number enhances by setting the hot surface at the lower part of the cavity. The vorticity pattern in cavity for different positions of hot and cold surfaces is demonstrated in Fig. 13. When the hot surface is in the upper half of cavity at the geometry 1 and 2, two vorticities are formed which one of them is smaller in left side and the other in right side of the cavity. However, when the hot surface is located in the lower part of the cavity at geometry 3 and 4, one vorticity with more strength is created in the enclosure which will result in the Nu enhancement.

To investigate the variation trend of Nu number versus porosity at different Rayleigh numbers, the graph presented in Fig. 14 is provided. As obviously shown, for all the cases, enhancing the buoyancy force coming from augmentation of Ra boosts average Nusselt number. In fact, decreasing porosity will lead in declining of convection heat transfer and Nu reduction. The isotherm line for various porosity are depicted in Fig. 15. Convection is strengthened by increasing porosity and isotherm lines are getting more affected by advection fluid flow and denser next to the hot wall.

The Nu number variation versus Ha number at different power law indexes is demonstrated in Fig. 16. Nu decreases almost 10.5%, 7.6% and 5.2% by increasing Ha number from 0.0 to 40.0 at viscosity power law index of 0.6, 1.0 and 1.4, respectively.

Fig. 17 provides isotherm lines for different power law indexes at φ=0.05, Da=0.001, Ra=1.5*10^5 and δ/L=0.2. It is noticed that the power-law index enhancement make the fluid isotherms density on the hotter wall to enhance. Actually, it reveals that the rise of power-law index augments the convection heat transfer in general. The impact is most evident in the isotherm near the upper left side of the enclosure where the enhancement in the power-law index induces the movement of the isotherm between the hot and cold walls to increase. The comparison between different power law indices in the isotherms elucidates that the Dilatant nanofluid (n>1) isotherms leans more toward the hot wall than the pseudoplastic nanofluid (n<1) and thus proves that heat transfer augments with enhancing power law index.

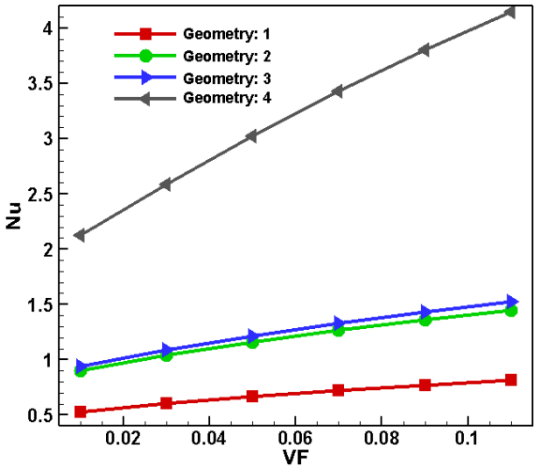

Fig. 12. The Nu variation vs. volume fraction of nanofluid with different positions of hot and cold surfaces at Da=0.001, Ra=1.5*10^6 and ε=0.75

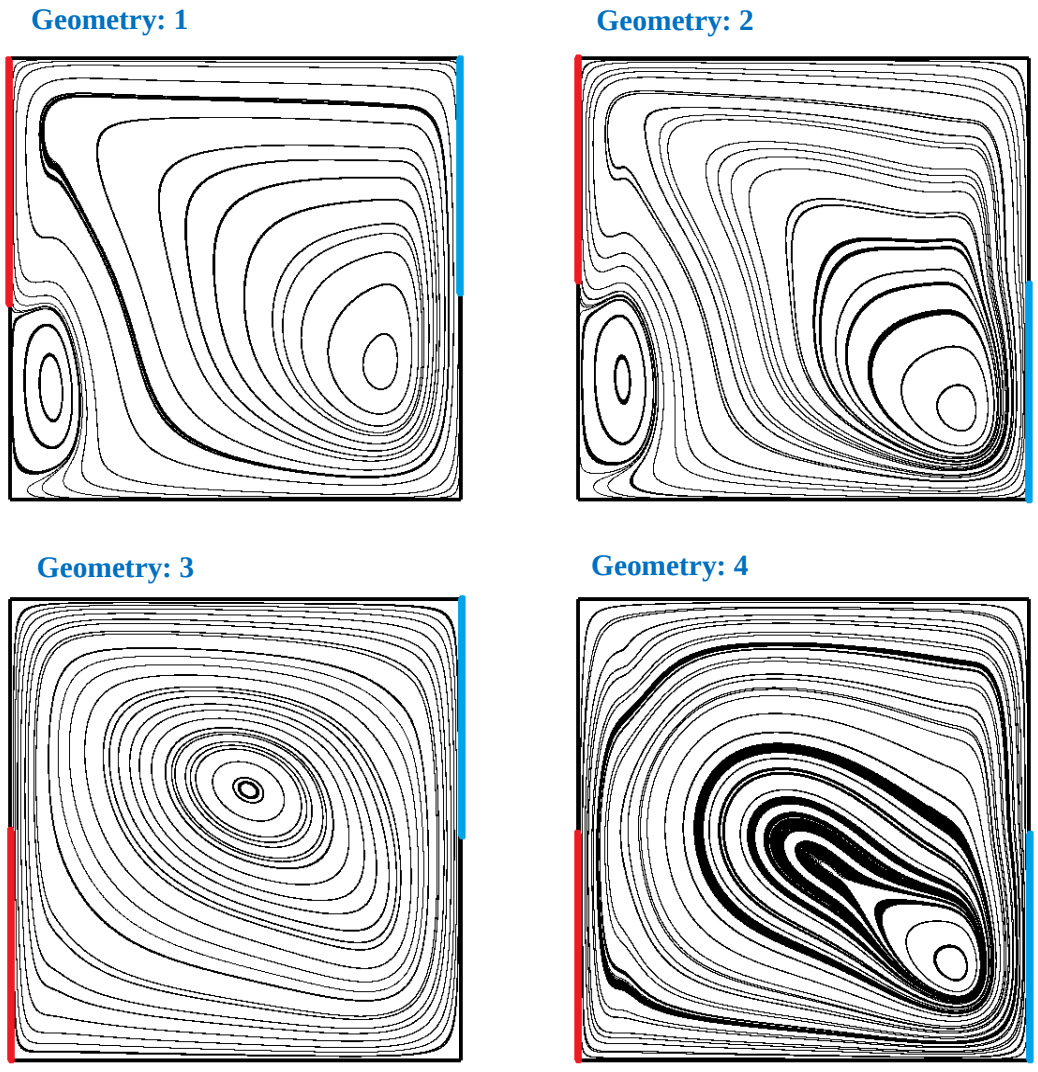

Fig. 13. The stream line at φ=0.01, Da=0.001, Ra=1.5*10^6 and ε=0.75 for different location of hot and cold surfaces

Table 3. The Nu variation vs. volume fraction of nanofluid with different positions of hot and cold surfaces at Da=0.001, Ra=1.5*10⁶ and ε=0.75

VF	0.01	0.03	0.05	0.07	0.09	0.11
Nu (Geomety 1)	0.529	0.601	0.664	0.720	0.769	0.813
Nu (Geomety 2)	0.903	1.039	1.161	1.269	1.364	1.447
Nu (Geomety 3)	0.941	1.087	1.215	1.329	1.431	1.523
Nu (Geomety 4)	2.126	2.584	3.022	3.429	3.804	4.144

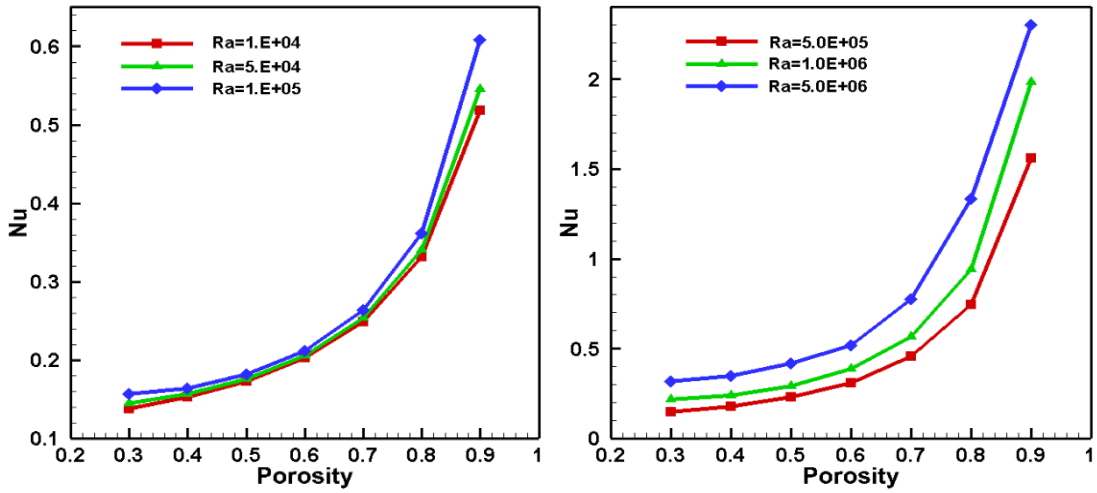

Fig. 14. The Nu number variation vs. porosity at φ=0.01, Da=0.001, Ra=1.5*10⁶ for different Ra numbers

Table 4. The Nu number variation vs. porosity at φ=0.01, Da=0.001, Ra=1.5*10⁶ for different Ra numbers

ε	0.3	0.4	0.5	0.6	0.7	0.8	0.9
Nu (Ra=1.E+4)	0.138	0.153	0.173	0.202	0.248	0.332	0.518
Nu (Ra=5.E+4)	0.145	0.157	0.176	0.205	0.257	0.341	0.545
Nu (Ra=1.E+5)	0.157	0.164	0.181	0.212	0.264	0.361	0.608
Nu (Ra=5.E+5)	0.171	0.180	0.230	0.310	0.456	0.746	1.562
Nu (Ra=1.E+6)	0.216	0.237	0.2916	0.388	0.567	0.941	1.985
Nu (Ra=5.E+6)	0.322	0.351	0.421	0.520	0.776	1.334	2.302

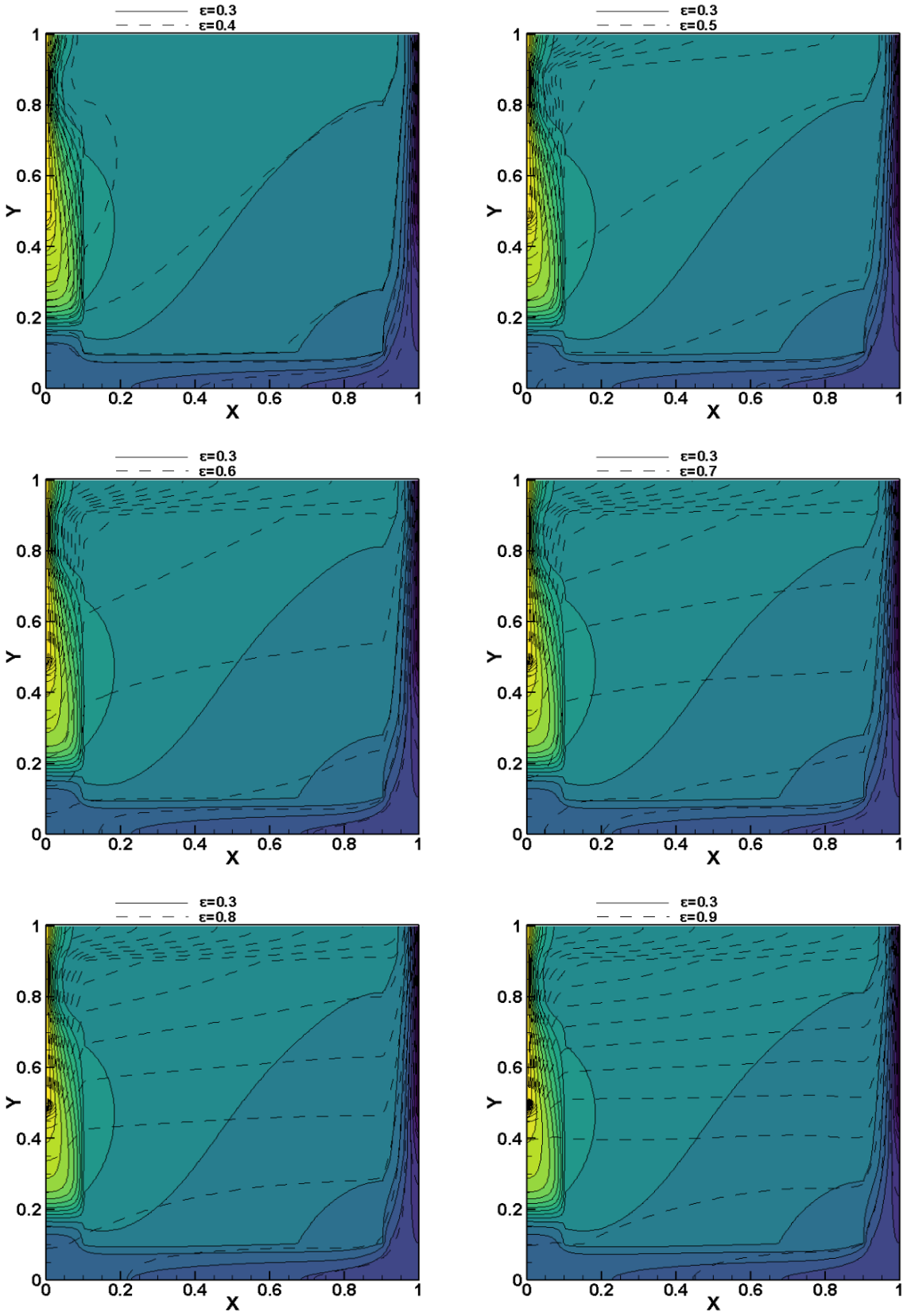

Fig. 15. Comparison of the isotherm lines at different porosities for φ=0.05, Da=0.001, Ra=1.5*10^5 and δ/L=0.2

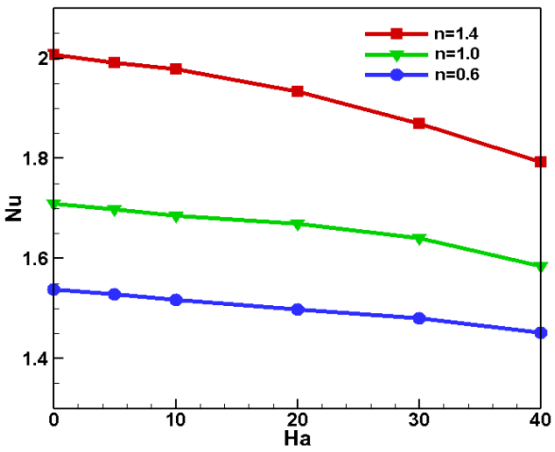

Fig. 16. Nu number variation vs. Ha number in different viscosity power law indexes at φ=0.05, Da=0.001, Ra=1.5*10^5 and δ/L=0.2

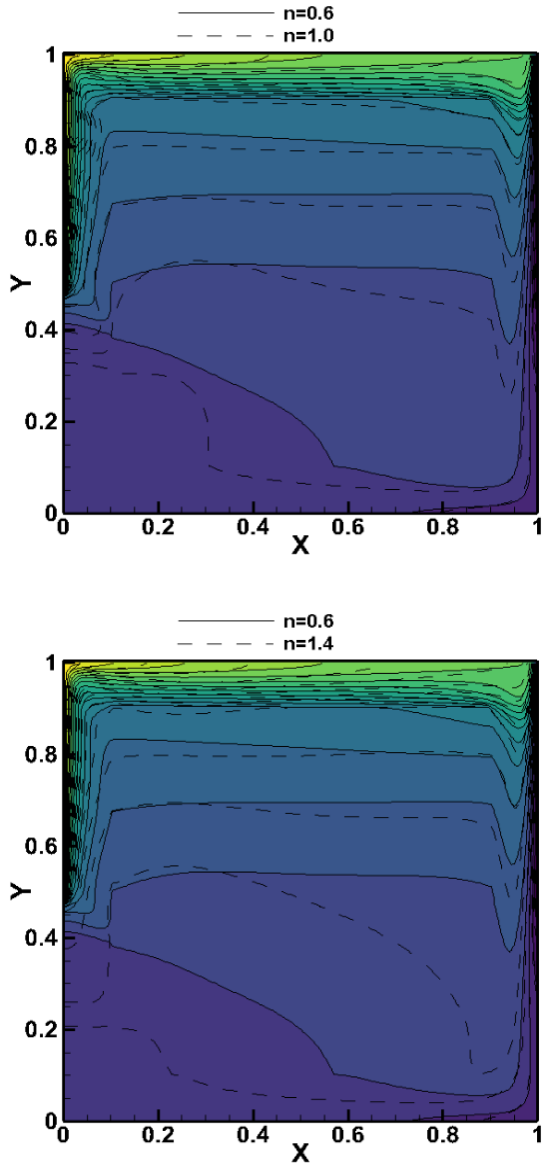

Fig. 17. Comparison of the isotherm lines at different viscosity power law indexes for φ=0.05, Da=0.001, Ra=1.5*105 and δ/L=0.2

Fig. 18 illustrates Nu number increases by enhancement of nanoparticle volume fraction. It reveals Nu increases almost 36%, 47% and 53% at inclination angle of 30^o, 0^o and −30^o by enhancing volume fraction from 0.02 to 0.12, respectively. Nanoparticle effect is more dominant at angle of −30^o. Because, in this situation, buoyancy forces boosts natural convection and this is supplemented by nanoparticle conductivity augmentation in nanofluid.

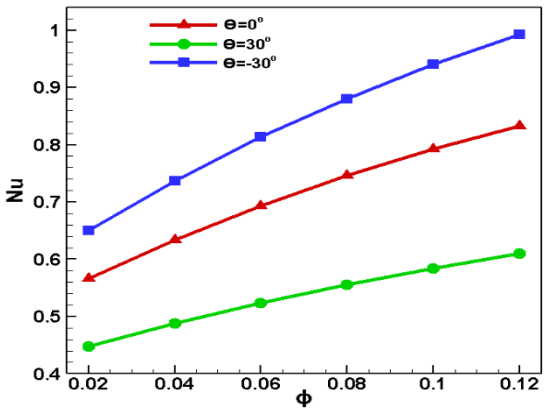

Fig. 18. Nu number vs. nanoparticle volume fraction at different angle of inclinations for ε=0.75, Da=0.001, Ra=1.5*10^5 and δ/L=0.2

The Bejan number is defined the ratio of heat transfer irreversibility to total irreversibility due to heat transfer and fluid friction. The variation of magnetic entropy generation and Be number is demonstrated in Fig. 19. Magnetic entropy generation and Be number enhances by increasing Da number. Convection heat transfer and fluid flow will be more dominant by augmentation of permeability and Da number and this will lead to more entropy generation by fluid flow and less entropy generation and irreversibility by magnetic field and convective heat transfer process.

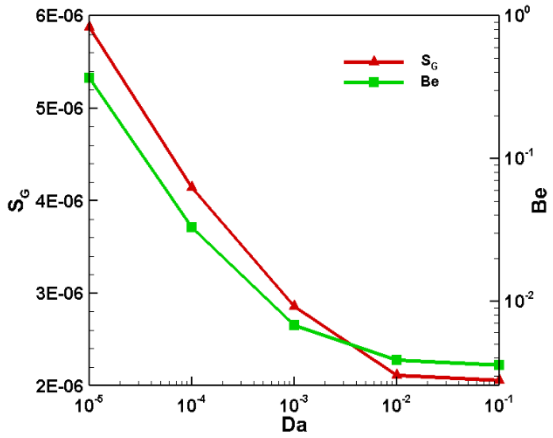

Fig. 19. The magnetic entropy production and Bejan number variation vs. Darcy number at at φ=0.05, δ/L=0.2, Ra=1.5*10^5 and ε=0.75

Table 5. Nu number vs. nanoparticle volume fraction at different angle of inclinations for ε=0.75, Da=0.001, Ra=1.5*10^5 and δ/L=0.2

φ	0.1	0.2	0.3	0.4	0.5	0.6
Nu (θ=0°)	0.566	0.633	0.693	0.745	0.792	0.833
Nu (θ=30°)	0.447	0.487	0.523	0.555	0.583722	0.609476
Nu (θ=-30°)	0.649	0.737	0.813	0.880	0.939825	0.992884

The contour of Be number versus Da number is also depicted in Fig. 20. In low Da number irreversibility spreads all over the region and it indicates a dominance of the heat transfer irreversibility over the fluid friction irreversibility. However, in higher Da number, fluid flow entropy generation is the main cause of irreversibility and Be number is substantially suppressed in fluid domain.

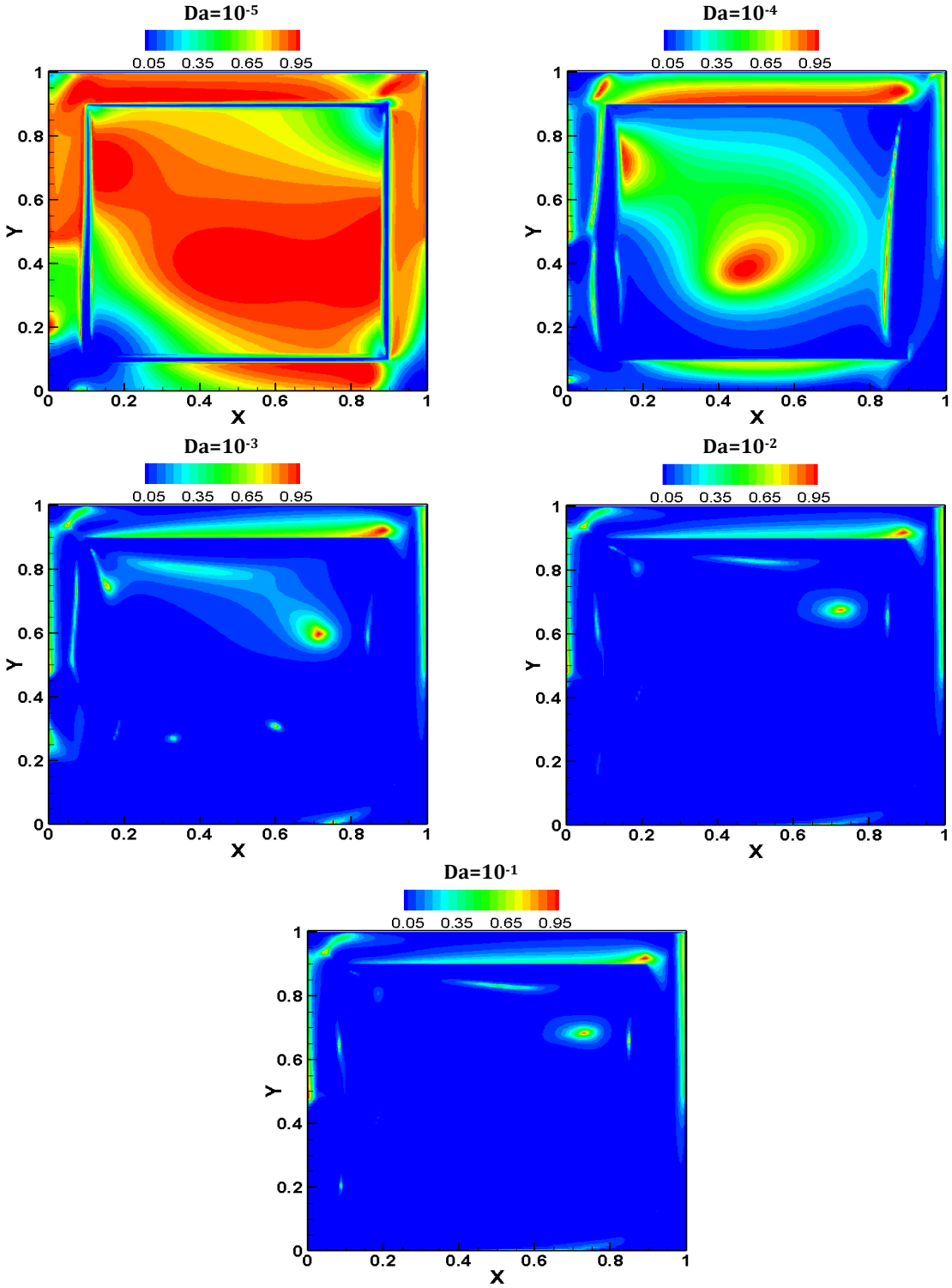

Fig. 20. Be number contours at different Da numbers for for ε=0.75, φ=0.05, Ra=1.5*10^5 and δ/L=0.2

At Fig. 21, fluid flow and magnetic field entropy generation decrease and heat transfer irreversibility and Be number rises by porous thickness ratio. It is obvious that Ra number reduces by increasing porous thickness ratio and natural convection decrease consequently and so that fluid flow friction entropy generation and magnetic field effect on irreversibility will diminish. However, temperature gradient enhances in solid wall especially in porous section and as a result entropy generation will increase as depicted in Fig. 22.

As it is seen in Fig. 23, Be number and thermal entropy generation increases with porosity. However, irreversibility due to fluid friction and magnetic field decreases. By increasing porosity fluid can flow more freely and therefore fluid friction reduces and this will result in SF reduction. Conversely, convection heat transfer is strengthened by increasing porosity and this will lead to enhancement of temperature gradient in the enclosure particularly in the middle zone and the upper porous section as revealed in Fig. 24.

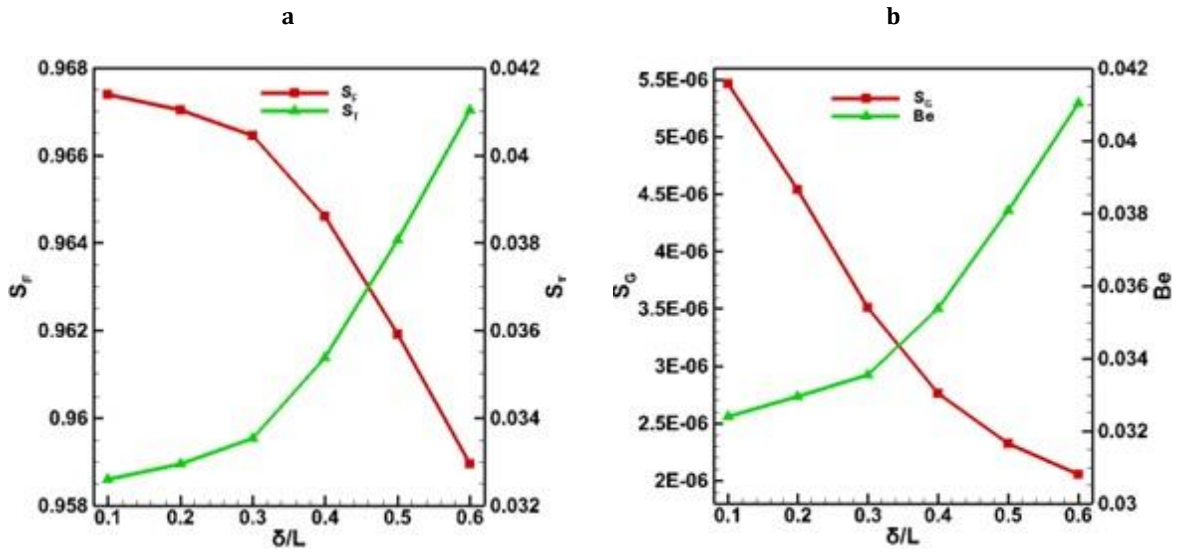

Fig. 21. The a) fluid flow and thermal entropy production and b) magnetic entropy production and Bejan number variation vs. thickness ratio at Da=0.001, φ=0.05, Ra=1.5*10^5 and ε=0.75

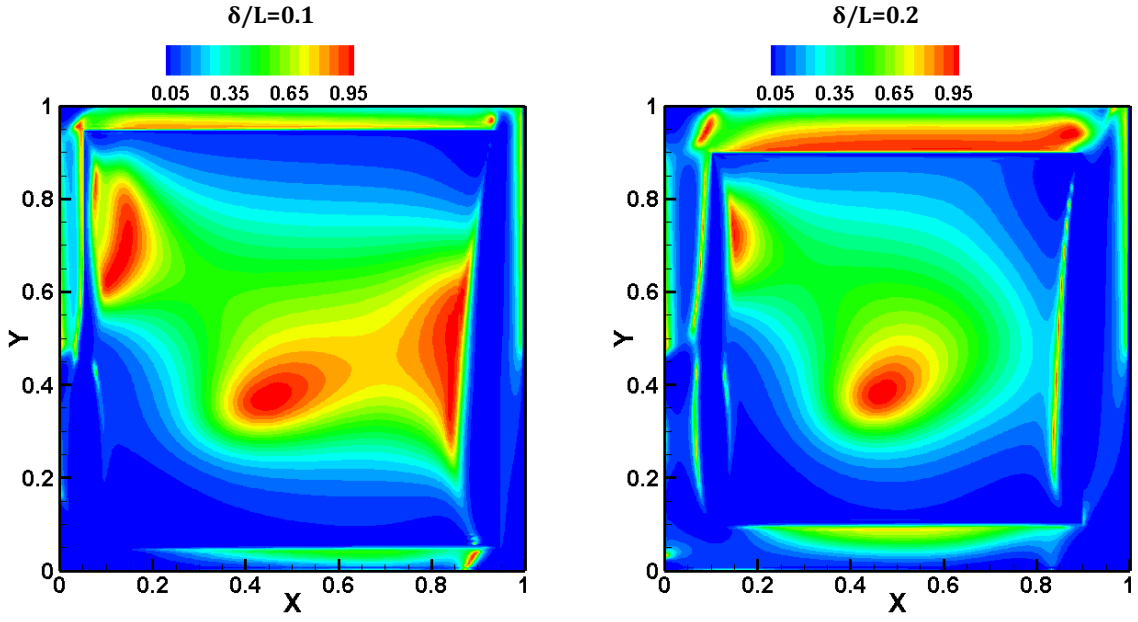

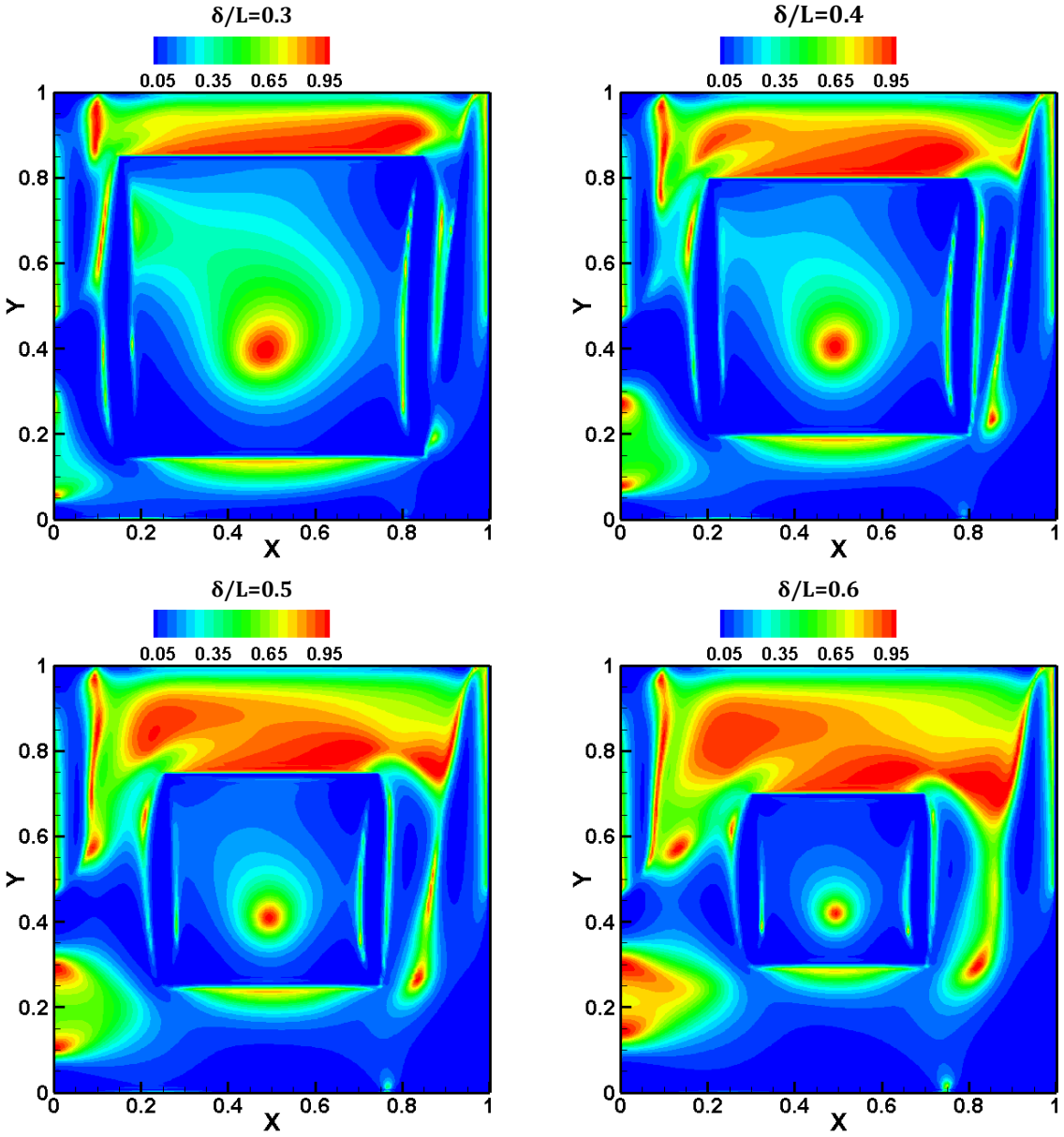

Fig. 22. Be number contours at different thickness ratios for ε=0.75, φ=0.05, Ra=1.5*10^5 and Da=0.001

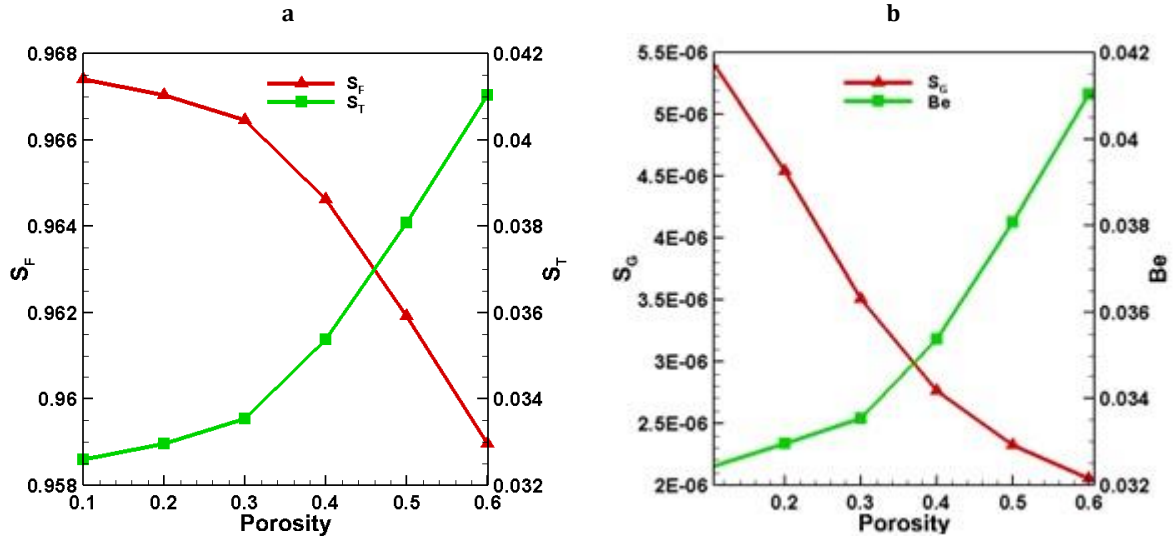

Fig. 23. The a) fluid flow and thermal entropy production and b) magnetic entropy production and Bejan number variation vs. porosity at Da=0.001, φ=0.05, Ra=1.5*10^5 and δ/L=0.2

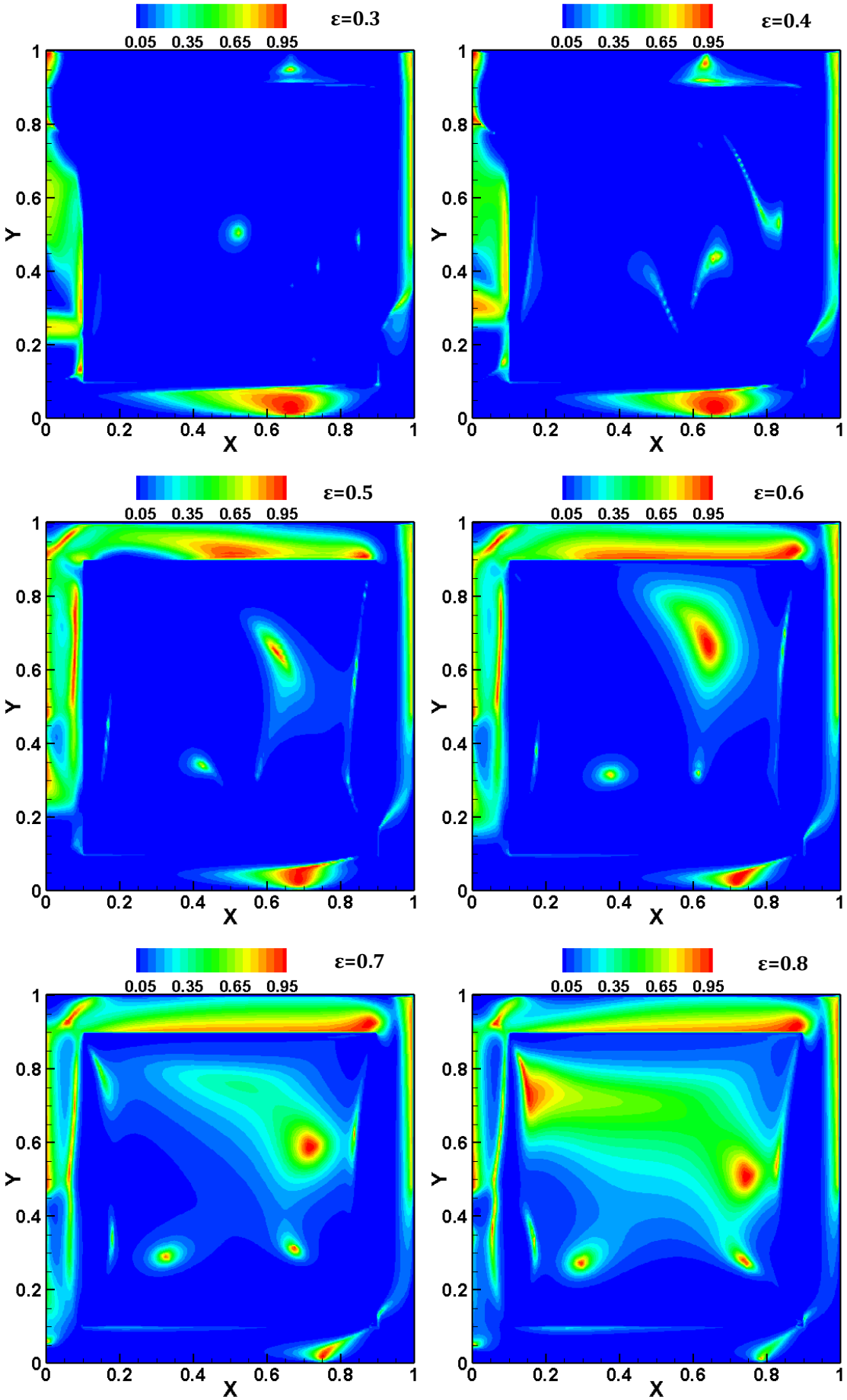

Fig. 24. Be number contours at different porosities for for δ/L=0.2, φ=0.05, Ra=1.5*10^5 and Da=0.001

5. Conclusion

In this study, MHD of hybrid Cu-Al_2O_3 non-Newtonian nanofluid with partially heated wall in an inclined partially porous cavity was investigated. The irreversibility and average Nusselt number were obtained by using CVFVM at the presence of magnetic field. The effect of main parameters such as porosity, porous thickness ratio, position of heated wall, Da number, Ha number and the angle of inclination was evaluated on the entropy generation and average Nu number. The important results can be summarized as follows:

1. Nu number increase almost 39%, 50% and 52% with enhancing porous media thickness from 0.1 to 0.6 at inclination angle of -30o, 0^o and 30^o, respectively.
2. The Nu number increases by setting the hot surface at the lower part of the cavity.
3. Convection heat transfer and fluid flow will be more dominant by augmentation of permeability and Da number and this will lead to more entropy production by fluid flow and less entropy production and irreversibility by magnetic field and convective heat transfer process.
4. Fluid flow and magnetic field entropy generation decrease and heat transfer irreversibility and Be number rises by porous thickness ratio.

Nomenclature

B	Magnetic field (T)
C_f	Specific heat at constant pressure (kJ/kg.K)
Da	Darcy number
Ha	Hartmann number($\mathrm{Ha} = \mathrm{BL}\sqrt{\sigma/\nu}$)
k	Heat conductivity (W/m.K)
L	Length of cavity (m)
n	Power-law index
N	The consistency coefficient
Nu	Nusselt number(Nu=hL/k)
p	Pressure (Pa)
Pr	Prandtl number(Pr=ν/α)
Re	Reynolds number(Re=UL/ν)
t	Time (s)
T	Temperature (K)
u	x-velocity (m/s)
v	y-velocity (m/s)
x, y	Cartesian coordinate (m)

Greek letters

ρ	Density (kg/m^3)
μ	Viscosity (Pa.s)
σ	The electrical conductivity (S/m)
φ	Volume fraction
τ	Shear stress (N/m^2)
ε	Porosity
θ	Angle (degree)

Subscripts

C	Cold
H	Hot
nf	Nanofluid

Funding Statement

This research did not receive any specific grant from funding agencies in the public, commercial, or not-for-profit sectors.

Conflicts of Interest

The author declares that there is no conflict of interest regarding the publication of this article.

References

[1] Cekmecelioglu, D., 2021. Convective heat transfer in food process engineering. Engineering principles of unit operations in food processing. Elsevier, pp. 315–344.

[2] Cordioli, M., Rinaldi, M. and Barbanti, D., 2016. Investigation and modelling of natural convection and conduction heat exchange: study on food systems with modified starch by means of computational fluid dynamics. International Journal of Food Science \& Technology. Wiley Online Library, 51(4), pp. 854–864.

[3] Omosebi, A. O. and Igbokoyi, A. O., 2016. Boundary effect on pressure behavior of Power-Law non-Newtonian fluids in homogeneous reservoirs. Journal of Petroleum Science and Engineering. Elsevier, 146, pp. 838–855. doi: 10.1016/j.petrol.2016.07.036.

[4] Nie, R. S. et al., 2018 Modeling the characteristics of Bingham porous-flow mechanics for a horizontal well in a heavy oil reservoir. Journal of Petroleum Science and Engineering. Elsevier B.V., 171, pp. 71–81. doi: 10.1016/j.petrol.2018.07.026.

[5] Kumar, A. and Saha, S. K., 2016. Energy and exergy analyses of medium temperature latent heat thermal storage with high

porosity metal matrix. Applied Thermal Engineering. Elsevier Ltd, 109, pp. 911–923. doi: 10.1016/j.applthermaleng.2016.04.161.

[6] Ouahouah, A. et al., 2021. Journal of Non-Newtonian Fluid Mechanics Natural convection within a non-uniformly heated cavity partly filled with a shear-thinning nanofluid and partly with air. Journal of Non-Newtonian Fluid Mechanics. Elsevier B.V., 289 (January), p. 104490. doi: 10.1016/j.jnnfm.2021.104490.

[7] Lamraoui, H., Mansouri, K. and Saci, R., 2019. Journal of Non-Newtonian Fluid Mechanics Numerical investigation on fluid dynamic and thermal behavior of a non-Newtonian Al2O3– water nanofluid flow in a confined impinging slot jet. Journal of Non-Newtonian Fluid Mechanics. Elsevier B.V., 265 (July 2018), pp. 11–27. doi: 10.1016/j.jnnfm.2018.12.011.

[8] Kang, J. et al., 2014. Journal of Non-Newtonian Fluid Mechanics Thermal instability of a nonhomogeneous power-law nanofluid in a porous layer with horizontal throughflow. Journal of Non-Newtonian Fluid Mechanics. Elsevier B.V., 213, pp. 50–56. doi: 10.1016/j.jnnfm.2014.09.006.

[9] Sheremet, M. A. and Pop, I., 2018. Effect of local heater size and position on natural convection in a tilted nanofluid porous cavity using LTNE and Buongiorno's models. Journal of Molecular Liquids. Elsevier B.V., 266, pp. 19–28. doi: 10.1016/j.molliq.2018.06.065.

[10] Jamaludin, A. et al., 2020. MHD mixed convection stagnation-point flow of Cu-Al2O3/water hybrid nanofluid over a permeable stretching/shrinking surface with heat source/sink. European Journal of Mechanics, B/Fluids. Elsevier Masson SAS., 84, pp. 71–80. doi: 10.1016/j.euromechflu.2020.05.017.

[11] Alsabery, A. I. et al., 2017. Effects of finite wall thickness and sinusoidal heating on convection in nanofluid-saturated local thermal non-equilibrium porous cavity. Physica A: Statistical Mechanics and its Applications. Elsevier B.V., 470, pp. 20–38. doi: 10.1016/j.physa.2016.11.107.

[12] Khan, Z. H. et al., 2020. Hydromagnetic flow of ferrofluid in an enclosed partially heated trapezoidal cavity filled with a porous medium', Journal of Magnetism and Magnetic Materials. Elsevier B.V., 499, p. 166241. doi: 10.1016/j.jmmm.2019.166241.

[13] Pekmen Geridonmez, B. and Oztop, H. F., 2019. Natural convection in a cavity filled with porous medium under the effect of a partial magnetic field. International Journal of Mechanical Sciences. Elsevier Ltd, 161–162, p. 105077. doi: 10.1016/j.ijmecsci.2019.105077.

[14] Toosi, M. H. and Siavashi, M., 2017. Two-phase mixture numerical simulation of natural convection of nanofluid flow in a cavity partially filled with porous media to enhance heat transfer. Journal of Molecular Liquids. Elsevier B.V, 238, pp. 553–569. doi: 10.1016/j.molliq.2017.05.015.

[15] Rodríguez-Núñez, K., Tabilo, E. and Moraga, N. O., 2019. Conjugate unsteady natural heat convection of air and non-Newtonian fluid in thick walled cylindrical enclosure partially filled with a porous media. International Communications in Heat and Mass Transfer. Elsevier, 108, p. 104304. doi: 10.1016/j.icheatmasstransfer.2019.104304.

[16] Sheikholeslami, M. and Vajravelu, K., 2017. Nanofluid flow and heat transfer in a cavity with variable magnetic field. Applied Mathematics and Computation, Elsevier Inc., 298, pp. 272–282. doi: 10.1016/j.amc.2016.11.025.

[17] Zhang, Y. et al., 2020. Flow and heat transfer simulation in a wall-driven porous cavity with internal heat source by multiple-relaxation time lattice Boltzmann method (MRT-LBM). Applied Thermal Engineering. Elsevier, 173(March), p. 115209. doi: 10.1016/j.applthermaleng.2020.115209.

[18] Sheremet, M. A. and Pop, I., 2015. Natural convection in a horizontal cylindrical annulus filled with a porous medium saturated by a nanofluid using Tiwari and Das' nanofluid model. European Physical Journal Plus, 130(6), pp. 1-12. doi: 10.1140/epjp/i2015-15107-4.

[19] Li, Z. et al., 2019. Nanofluid heat transfer in a porous duct in the presence of Lorentz forces using the lattice Boltzmann method. European Physical Journal Plus, 134(1). doi: 10.1140/epjp/i2019-12406-8.

[20] Rajarathinam, M., Nithyadevi, N. and Chamkha, A. J., 2018. Heat transfer enhancement of mixed convection in an inclined porous cavity using Cu-water nanofluid. Advanced Powder Technology. The Society of Powder Technology Japan, 29(3), pp. 590–605. doi: 10.1016/j.apt.2017.11.032.

[21] Vijaybabu, T. R. and Dhinakaran, S., 2019. MHD Natural convection around a permeable triangular cylinder inside a square enclosure filled with Al2O3 –H2O nanofluid: An LBM study. International Journal of Mechanical Sciences. Elsevier Ltd, 153–154, pp. 500–516. doi: 10.1016/j.ijmecsci.2019.02.003.

[22] Gibanov, N. S. et al., 2017. Effect of uniform inclined magnetic field on mixed convection in a lid-driven cavity having a horizontal porous layer saturated with a ferrofluid. International Journal of Heat and Mass Transfer. Elsevier Ltd, 114, pp. 1086–1097. doi:10.1016/j.ijheatmasstransfer.2017.07.001.

[23] Ellahi, R. et al., 2023. Natural convection nanofluid flow with heat transfer analysis of carbon nanotubes–water nanofluid inside a vertical truncated wavy cone. Mathematical Methods in the Applied Sciences, 46(10), pp. 11303–11321. doi: 10.1002/mma.7281.

[24] Ellahi, R., 2013. The effects of MHD and temperature dependent viscosity on the flow of non-Newtonian nanofluid in a pipe: Analytical solutions. Applied Mathematical Modelling. Elsevier Inc., 37(3), pp. 1451–1467. doi: 10.1016/j.apm.2012.04.004.

[25] Aneja, M., Chandra, A. and Sharma, S., 2020. Natural convection in a partially heated porous cavity to Casson fluid. International Communications in Heat and Mass Transfer. Elsevier, 114, p. 104555. doi: 10.1016/j.icheatmasstransfer.2020.104555.

[26] Astanina, M. S. et al., 2018. MHD natural convection and entropy generation of ferrofluid in an open trapezoidal cavity partially filled with a porous medium. International Journal of Mechanical Sciences. Elsevier Ltd, 136(December 2017), pp. 493–502. doi: 10.1016/j.ijmecsci.2018.01.001.

[27] Selimefendigil, F. and Öztop, H. F., 2020b. Magnetohydrodynamics forced convection of nanofluid in multi-layered U-shaped vented cavity with a porous region considering wall corrugation effects. International Communications in Heat and Mass Transfer, Elsevier, 113, p. 104551. doi: 10.1016/j.icheatmasstransfer.2020.104551.

[28] Khan, A. A. et al., 2023. Heat transmission in Darcy-Forchheimer flow of Sutterby nanofluid containing gyrotactic microorganisms. International Journal of Numerical Methods for Heat \& Fluid Flow. Emerald Publishing Limited, 33(1), pp. 135–152.

[29] Zeeshan, A. et al., 2023. Hydromagnetic flow of two immiscible nanofluids under the combined effects of Ohmic and viscous dissipation between two parallel moving plates. Journal of Magnetism and Magnetic Materials. Elsevier, 575, p. 170741.

[30] Kole, M. and Dey, T. K., 2010. Thermal conductivity and viscosity of Al2O3 nanofluid based on car engine coolant. Journal of Physics D: Applied Physics, 43(31). doi: 10.1088/0022-3727/43/31/315501.

[31] Yu, W. and Xie, H., 2012. A review on nanofluids: Preparation, stability mechanisms, and applications. Journal of Nanomaterials, 2012. doi: 10.1155/2012/435873.

[32] Vafai, K., 2010. Porous media: applications in biological systems and biotechnology. CRC Press.

[33] Selimefendigil, F. and Öztop, H. F., 2020a. Effects of conductive curved partition and magnetic field on natural convection and entropy generation in an inclined cavity filled with nanofluid. Physica A: Statistical Mechanics and its Applications. Elsevier B.V., 540, p. 123004. doi: 10.1016/j.physa.2019.123004.

[34] Bin-Nun, U. and Manitakos, D., 2004. Low cost and high performance screen laminate regenerator matrix. Cryogenics, 44(6–8), pp. 439–444. doi:10.1016/j.cryogenics.2004.03.015.

[35] Kefayati, G. R., 2016 Simulation of heat transfer and entropy generation of MHD natural convection of non-Newtonian nanofluid in an enclosure, International Journal of Heat and Mass Transfer. Elsevier Ltd, 92, pp. 1066–1089. doi: 10.1016/j.ijheatmasstransfer.2015.09.078.

[36] Zhang, S., Zhao, X. and Bayyuk, S., 2014. Generalized formulations for the rhie-chow interpolation. Journal of Computational Physics. Elsevier Inc., 258, pp. 880–914. doi: 10.1016/j.jcp.2013.11.006.

[37] Kardgar, A. and Jafarian, A., 2016. Numerical investigation of oscillating conjugate heat transfer in pulse tubes. Applied Thermal Engineering. Elsevier Ltd, 105, pp. 557–565. doi:10.1016/j.applthermaleng.2016.03.045.

[38] Ferziger, J. H., Peric, M. and Leonard, A.,

2020. Computational Methods for Fluid Dynamics, springer. doi: 10.1063/1.881751.

[39] Kardgar, A. and Jafarian, A., 2020. Numerical simulation of turbulent oscillating flow in porous media. Scientia Iranica. doi:10.24200/SCI.2020.52521.2788.

[40] Khanafer, K., Vafai, K. and Lightstone, M., 2003. Buoyancy-driven heat transfer enhancement in a two-dimensional enclosure utilizing nanofluids. International Journal of Heat and Mass Transfer, 46(19), pp. 3639–3653. doi: 10.1016/S0017-9310(03)00156-X.

[41] Krane, R. and Jessee, J., 1983. Some Detailed Field Measurement for a Natural Convection Flow in a Vertical Square Enclosure. in Proceedings of the First ASME-JSME Thermal Engineering Joint Conference, pp. 323–329.